CGC/saturation approach: A new impact-parameter-dependent model in the next-to-leading order of perturbative QCD

Carlos Contreras,[1,*] Eugene Levin,[1,2,†] Rodrigo Meneses,[3,‡] and Irina Potashnikova[1,§]

[1]*Departemento de Física, Universidad Técnica Federico Santa María, and Centro Científico- Tecnológico de Valparaíso, Avda. Espana 1680, Casilla 110-V, Valparaíso, Chile*

[2]*Department of Particle Physics, School of Physics and Astronomy, Raymond and Beverly Sackler Faculty of Exact Science, Tel Aviv University, Tel Aviv 69978, Israel*

[3]*Escuela de Ingeniería Civil, Facultad de Ingeniería, Universidad de Valparaíso, Avda Errazuriz 1834, Valparaíso, Chile*

(Received 25 July 2016; published 23 December 2016)

This paper is the first attempt to build a color glass condensate/saturation model based on the next-to-leading-order (NLO) corrections to linear and nonlinear evolution in QCD. We assume that the renormalization scale is the saturation momentum and find that the scattering amplitude has geometric scaling behavior deep in the saturation domain with the explicit formula of this behavior at large $\tau = r^2 Q_s^2$. We build a model that includes this behavior, as well as the known ingredients: (i) the behavior of the scattering amplitude in the vicinity of the saturation momentum, using the NLO Balitsky-Fadin-Kuraev-Lipatov kernel, (ii) the pre-asymptotic behavior of $\ln(Q_s^2(Y))$, as a function of Y, and (iii) the impact parameter behavior of the saturation momentum, which has exponential behavior $\propto \exp(-mb)$ at large b. We demonstrate that the model is able to describe the experimental data for the deep inelastic structure function. Despite this, our model has difficulties that are related to the small value of the QCD coupling at $Q_s(Y_0)$ and the large values of the saturation momentum, which indicate the theoretical inconsistency of our description.

DOI: 10.1103/PhysRevD.94.114028

I. INTRODUCTION

This paper is the next step (see Ref. [1]) in our attempt to find an approach, based on color glass condensate (CGC)/saturation effective theory for high-energy QCD (see Ref. [2] for a review), which includes the impact parameter dependence of the scattering amplitude. Unfortunately, at the moment, our efforts reduce to building a model which incorporates the main features of the solution of the CGC/saturation equations, and also contains a number of phenomenological parameters for the nonperturbative QCD description of the large impact parameter dependence of the scattering amplitude.

We are doomed to build models to introduce the main features of the CGC/saturation approach, since the CGC/saturation equations do not reproduce the correct behavior of the scattering amplitude at large impact parameters (see Refs. [3,4]). Such a failure leads to the conclusion that we cannot trust the solution of the CGC/saturation equations, without the long-distance nonperturbative corrections at large impact parameters.

Indeed, for the scattering of a dipole with size r with the nucleus, the CGC/saturation equations [5,6] (see Eq. 2.6 in Ref. [7]) can be rewritten for $N(r, Y, Q_T = 0) = \int d^2b N(r, Y, b)$ using the natural assumption that $r \ll R_A$, where R_A is the size of the nucleus. $N(r, Y, Q_T = 0)$ is the infrared-safe observable in perturbative QCD and, hence, we can expect that nonperturbative corrections for it will be small. The radius of the dipole increases with energy growth, but from high-energy phenomenology we learned that this increase is of the order $\alpha'_{IP} Y \ll R_A$ for $Y \leq 40$. Implicitly, we assume that the nonperturbative corrections change the power-like increase with energy of the interaction radius (which follows from perturbative QCD [3,4]) to a logarithmic one: we believe that this change does not lead to the violation of the CGC/saturation equations.

However, for the interaction with a proton we do not even have this rather weak argument, and for a hadron target we anticipate large corrections to the CGC/saturation equations. Real progress in the theoretical understanding of the confinement of quarks and gluons has not yet been made, and as a result, we do not know how to change the CGC/saturation equations to incorporate confinement. We have to build a model which includes both theoretical knowledge that stems from the CGC/saturation equations, and the phenomenological large-b behavior, which do not contradict theoretical restrictions [8,9].

Numerous attempts have been made over the past two decades (see Refs. [1,10–29]) to build such models. Therefore, we clarify, in the Introduction, the aspects of our model which are different.

*carlos.contreras@usm.cl
†leving@post.tau.ac.il, eugeny.levin@usm.cl
‡rodrigo.meneses@uv.cl
§irina.potashnikova@usm.cl

The main difference of this paper from others, is that we use the nonlinear Balitsky-Kovchegov (BK) equation in the next-to-leading order (NLO) of perturbative QCD, that has been proven in Refs. [30–32]. The form of the BK equation in the NLO shows that we can apply the method, suggested in Ref. [33], for determining the behavior of the solution to the BK equation deep inside the saturation region. This behavior in the NLO is given in this paper. It shows geometric scaling behavior as in the leading order of perturbative QCD, for the renormalization scale which is equal to the saturation momentum Q_s.

We only introduce the nonperturbative impact parameter behavior in the saturation momentum, accordingly to the spirit of the geometric scaling behavior of the scattering amplitude [34,35], and to the semiclassical solution to the CGC/saturation equations [12]. Similar assumptions for the nonperturbative b behavior of the scattering amplitude, are typical for most models on the market (see Refs. [17–21,24,29]). In the choice of the b behavior we follow the procedure, suggested in Ref. [1]:

$$Q_s^2(b,Y) \propto (S(b,m))^{\frac{1}{\bar{\gamma}}} \tag{1}$$

where $S(b)$ is the Fourier image of $S(Q_T) = 1/(1+\frac{Q_T^2}{m^2})^2$ and the value of $\bar{\gamma}$ will be discussed below. Such b dependence results in the large-b dependence of the scattering amplitude, in the vicinity of the saturation scale which is proportional to $\exp(-mb)$ at $b \gg 1/m$, in accordance with the Froissart theorem [8]. In addition, we reproduce the large-Q_T dependence of this amplitude proportional to Q_T^{-4} which follows from the perturbative QCD calculation [9].

In building our model we follow the strategy, suggested in Ref. [14], which consists of matching the behavior of the scattering dipole amplitude deep in the saturation domain, that is found using the method of Ref. [33], and the behavior of the scattering amplitude in the vicinity of the saturation scale [2,36,37]. In this paper, we follow the procedure of Refs. [1,38] which allows us to combine the exact form of the solution inside the saturation domain and in the vicinity of the saturation scale. In Refs. [10–29] only the characteristic behavior of the solution but not the exact form for it, was used.

We find the behavior of the amplitude in the vicinity of the saturation scale, using the NLO corrections to the Balitsky-Fadin-Kuraev-Lipatov (BFKL) Pomeron, calculated in Ref. [39] and the resummation, suggested in Ref. [40]. Such behavior has been discussed in Refs. [41,42]. In searching the parameters of the amplitude we use the procedure,[1] suggested in Ref. [42], for the full NLO kernel [40] as it has been explored in Ref. [41].

[1]We note that this procedure is quite different from the one, used in Ref. [41]. It is worth mentioning that we do not reproduce the result of Ref. [41] for the energy dependence of the saturation scale, but we are in agreement with the estimates of Ref. [42] if we apply our calculation to their simplified NLO kernel.

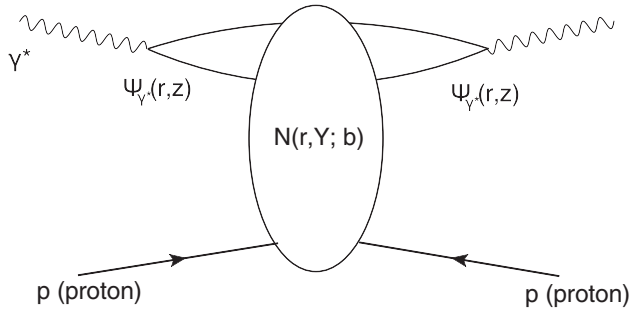

FIG. 1. The graphic representation of Eq. (2) for the scattering amplitude. $Y = \ln(1/x_{Bj})$ and r is the size of the interacting dipole. z denotes the fraction of energy that is carried by one quark. b denotes the impact parameter of the scattering amplitude.

II. THEORETICAL INPUT

A. General formula

The general formula for deep inelastic processes takes the form (see Fig. 1 and Ref. [2] for the review and references therein)

$$N(Q,Y;b) = \int \frac{d^2r}{4\pi}\int_0^1 dz |\Psi_{\gamma^*}(Q,r,z)|^2 N(r,Y;b) \tag{2}$$

where $Y = \ln(1/x_{Bj})$ and x_{Bj} is the Bjorken x. z is the fraction of energy carried by the quark. Q is the photon virtuality. b denotes the impact parameter of the scattering amplitude.

Equation (2) splits the calculation of the scattering amplitude into two stages: the calculation of the wave functions, and estimates of the dipole scattering amplitude.

B. Saturation momentum in the NLO

It is well known that the energy dependence of the saturation momentum can be found from the solution of the linear BFKL equation [34,36,37,43,44]. In the leading-order BFKL equation the saturation momentum Q_s at large values of rapidity has the following form:

$$Q_s^2 \propto e^{\lambda Y} \quad \text{where } \lambda = \bar{\alpha}_S \frac{\chi(\gamma_{cr})}{1-\gamma_{cr}} \quad \text{and}$$
$$\chi^{LO}(\gamma) = 2\psi(1) - \psi(\gamma) - \psi(1-\gamma) \tag{3}$$

where $\psi(z)$ is the digamma function. γ_{cr} is the solution of the equation

$$\frac{\chi(\gamma_{cr})}{1-\gamma_{cr}} = \left|\frac{d\chi(\gamma_{cr})}{d\gamma_{cr}}\right|. \tag{4}$$

In the NLO, the spectrum of the BFKL equation has been found in Ref. [39] and it has the following form:

$$\omega(\gamma) = \bar{\alpha}_S \chi^{LO}(\gamma) + \bar{\alpha}_S^2 \chi^{\rm NLO}(\gamma). \tag{5}$$

The explicit form of $\chi^{\rm NLO}(\gamma)$ is given in Ref. [39] (see Appendix A). However, $\chi^{\rm NLO}(\gamma)$ turns out to be singular at

$\gamma \to 1$, $\chi^{\rm NLO}(\gamma) \propto 1/(1-\gamma)^3$. Such singularities indicate that we have to calculate higher-order corrections to obtain a reliable result. The procedure to resum high-order corrections was suggested in Ref. [40]. The resulting spectrum of the BFKL equation in the NLO, can be found from the solution of the following equation [40,41]:

$$\omega = \bar{\alpha}_S\left(\chi_0(\omega,\gamma) + \omega\frac{\chi_1(\omega,\gamma)}{\chi_0(\omega,\gamma)}\right) \tag{6}$$

where

$$\chi_0(\omega,\gamma) = \chi^{LO}(\gamma) - \frac{1}{1-\gamma} + \frac{1}{1-\gamma+\omega} \tag{7}$$

and

$$\chi_1(\omega,\gamma) = \chi^{\rm NLO}(\gamma) + F\left(\frac{1}{1-\gamma} - \frac{1}{1-\gamma+\omega}\right) + \frac{A_T(\omega)-A_T(0)}{\gamma^2} + \frac{A_T(\omega)-b}{(1-\gamma+\omega)^2} - \frac{A_T(0)-b}{(1-\gamma)^2}. \tag{8}$$

The functions $\chi^{\rm NLO}(\gamma)$ and $A_T(\omega)$ as well as the constants (F and b) are presented in Appendix A.

Denoting the solution of Eq. (6) as $\omega^{\rm NLO}(\gamma)$ we see that Eq. (4) for γ_{cr} takes the form

$$\frac{\omega^{\rm NLO}(\gamma_{cr})}{1-\gamma_{cr}} = \left|\frac{d\omega^{\rm NLO}(\gamma_{cr})}{d\gamma_{cr}}\right|. \tag{9}$$

This equation was first derived in Ref. [43] in the semiclassical approximation for the dipole scattering amplitude. In this approximation the amplitude appears as the wave packet and Eq. (9) is the condition that the phase velocity of this wave packet is equal to the group velocity. This condition determines the special line (critical line) which gives the saturation scale. In Refs. [34,42] Eq. (9) was derived beyond the semiclassical approximation.

To find $\omega^{\rm NLO}(\gamma_{cr})$ and γ_{cr} we do not need to solve Eq. (5) explicitly. We can solve the system of two equations:

$$\omega_{cr} = \bar{\alpha}_S\left(\chi_0(\omega_{cr},\gamma_{cr}) + \omega\frac{\chi_1(\omega_{cr},\gamma_{cr})}{\chi_0(\omega_{cr},\gamma_{cr})}\right),$$
$$\frac{\omega_{cr}}{1-\gamma_{cr}} = \bar{\alpha}_S\left(\chi_0(\omega_{cr},\gamma_{cr}) + \omega\frac{\chi_1(\omega_{cr},\gamma_{cr})}{\chi_0(\omega_{cr},\gamma_{cr})}\right)'_\gamma \Big/ \left(1 - \bar{\alpha}_S\left(\chi_0(\omega_{cr},\gamma_{cr}) + \omega\frac{\chi_1(\omega_{cr},\gamma_{cr})}{\chi_0(\omega_{cr},\gamma_{cr})}\right)'_\omega\right) \tag{10}$$

where $\omega_{cr} \equiv \omega^{\rm NLO}(\gamma_{cr})$. In Fig. 2 we plot the solution to this set of equations. One can see that both γ_{cr} and λ differ from the leading-order estimates.

Figure 3 shows the solution of Eq. (6) in the form $\gamma = \gamma(\omega)$. One can see that $\gamma = \gamma(\omega) \to 0$ at $\omega \to 1$. This property means that we have energy conservation in the NLO, while in the LO $\gamma \propto \bar{\alpha}_S \neq 0$ at $\omega \to 0$, indicating the energy violation of the order of $\bar{\alpha}_S$.

The simple energy (rapidity) dependence of Eq. (3) only holds at large values of Y. The first two corrections lead to the following expression:

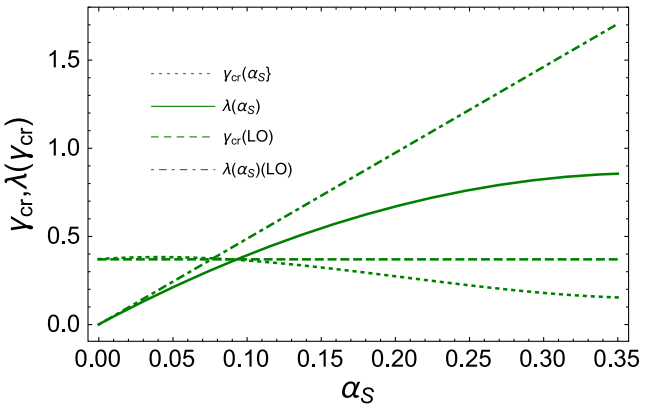

FIG. 2. $\lambda(\gamma_{cr})$ and γ_{cr} versus α_S.

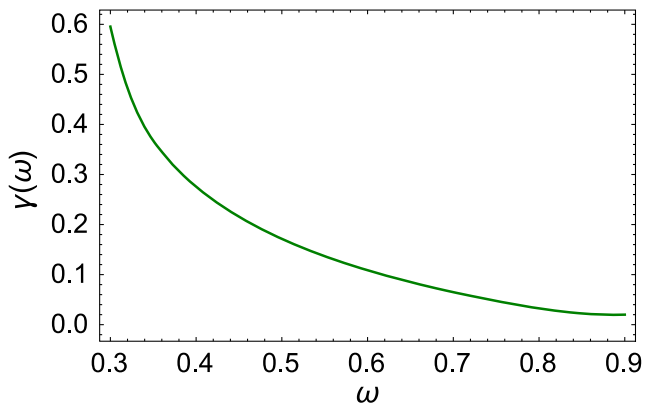

FIG. 3. γ versus ω for $\bar{\alpha}_S = 0.15$.

$$\ln\left(Q_s^2(Y)/Q_s^2(Y_0,b)\right)=\lambda^{\rm eff}(\bar{\alpha}_S,Y,Y_0)(Y-Y_0)$$
$$=\lambda(\gamma_{cr})(Y-Y_0)-\frac{3}{2(1-\gamma_{cr})}\ln(Y/Y_0)-\frac{3}{(1-\gamma_{cr})^2}\sqrt{\frac{2\pi}{\omega''(\gamma_{cr})}}\left(\frac{1}{\sqrt{Y}}-\frac{1}{\sqrt{Y_0}}\right)+\mathcal{O}\left(\frac{1}{Y}\right) \quad (11)$$

where $\omega''(\gamma_{cr})=d^2\omega(\gamma)/(d\gamma)^2$ at $\gamma=\gamma_{cr}$, and the values of $\lambda(\gamma_{cr})$ and γ_{cr} have been discussed above. Y_0 is the value of the rapidity from which we start the evolution. The first term was found in Ref. [43], the second in Ref. [37] and the third in Ref. [44]. In Fig. 4 $\ln\left(Q_s(b,Y)/Q_s(b,Y=Y_0)\right)$ is plotted at different values of $\bar{\alpha}_S$ in the region of $Y\leq 12$ where the most experimental data are available. In this plot we take into account that the running QCD coupling has to be taken at the scale $Q_s(Y)$ as we will argue in the next section, or in other words we use

$$\bar{\alpha}_S(Q_s)\frac{\bar{\alpha}_{S0}}{1+\bar{\alpha}_{S0}b\lambda_{cr}(Y-Y_0)} \quad (12)$$

where $\bar{\alpha}_{S0}=\bar{\alpha}_S(Q_0)$ is the QCD coupling at the scale $Q_0=Q_s(Y=Y_0)$ [see Eq. (26)].

One can see that the corrections to $\ln\left(Q_s(b,Y)/Q_s(b,Y=Y_0)\right)=\lambda_{cr}(Y-Y_0)$ are essential and they lead to $\lambda^{\rm eff}\approx 0.7\lambda_{cr}$. However, they turn out to be smaller than what was estimated in Ref. [41], perhaps because the last term in Eq. (11) was not taken into account.

Equation (11) shows that while we know the energy dependence theoretically, the value of $Q_s^2(Y_0,b)$ is our phenomenological input which we will discuss below.

C. Scattering amplitude in the vicinity of the saturation scale

In the region where $r^2Q_s^2(Y,b)\approx 1$ (in the vicinity of the saturation scale) the scattering amplitude has a well-known behavior [2,36,37]

$$N(r,Y;b)=N_0(r^2Q_s^2(b))^{1-\gamma_{cr}} \quad (13)$$

where γ_{cr} is the solution to Eq. (10).

The amplitude of Eq. (13) shows a geometric scaling behavior as a function of one variable $\tau=r^2Q_s^2(b)$. Such behavior arises inside the saturation region [33,34] where $\tau\geq 1$. However, it actually holds outside of the saturation region for $\tau\leq 1$ [36]. In Ref. [36] it is shown that the first corrections due to a violation of the geometric scaling behavior, can be taken into account by replacing $1-\gamma_{cr}$ in Eq. (13) by the following expression:

$$1-\gamma_{cr}\to 1-\gamma_{cr}-\frac{1}{2\kappa\lambda Y}\ln\left(r^2Q_s^2(b)\right) \quad (14)$$

where $\lambda=\bar{\alpha}_S\chi(\gamma_{cr})/(1-\gamma_{cr})$ and $\kappa=\chi''(\gamma_{cr})/\chi'(\gamma_{cr})$.

D. The scattering amplitude deep inside the saturation region [$r^2Q^2(b,Y)\gg 1$]

The nonlinear Balitsky-Kovchegov equation has been derived in the NLO, and it takes the form [30,31]

$$\frac{dS_{12}}{dY}=\frac{\bar{\alpha}_S}{2\pi}\int d^2x_3\frac{x_{12}^2}{x_{13}^2x_{23}^2}\left\{1+\bar{\alpha}_S b\left(\ln x_{12}^2\mu^2-\frac{x_{13}^2-x_{23}^2}{x_{12}^2}\ln\frac{x_{13}^2}{x_{23}^2}\right)+\bar{\alpha}_S\left(\frac{67}{36}-\frac{\pi^2}{12}-\frac{5}{18}\frac{N_f}{N_c}-\frac{1}{2}\ln\frac{x_{13}^2}{x_{12}^2}\ln\frac{x_{23}^2}{x_{12}^2}\right)\right\}(S_{13}S_{32}-S_{12})$$
$$+\frac{\bar{\alpha}_S^2}{8\pi^2}\int\frac{d^2x_3d^2x_4}{x_{34}^4}\left\{-2+\frac{x_{13}^2x_{24}^2+x_{14}^2x_{23}^2-4x_{12}^2x_{34}^2}{x_{13}^2x_{24}^2-x_{14}^2x_{23}^2}\ln\frac{x_{13}^2x_{24}^2}{x_{14}^2x_{23}^2}+\frac{x_{12}^2x_{34}^2}{x_{13}^2x_{24}^2}\left(1+\frac{x_{12}^2x_{34}^2}{x_{13}^2x_{24}^2-x_{14}^2x_{23}^2}\right)\ln\frac{x_{13}^2x_{24}^2}{x_{14}^2x_{23}^2}\right\}$$
$$\times(S_{13}S_{34}S_{42}-S_{13}S_{32}). \quad (15)$$

In Eq. (15) $x_{ik}=\boldsymbol{x}_i-\boldsymbol{x}_j$, μ is the renormalization scale for the running QCD coupling and all other constants are defined in Appendix A. S_{ij} is the S matrix for scattering of a dipole of size x_{ij}, with the target.

One can see that in the region where $S_{ij}\to 0$, all terms except the first one, which is proportional to S_{12}, are small and can be neglected. In other words, in the region where $S_{12}\gg S_{13}S_{32}\gg S_{13}S_{34}S_{42}$ we can reduce Eq. (15) to the following linear equation [33]:

$$\frac{dS_{12}}{dY}=-\frac{\bar{\alpha}_S}{2\pi}\int d^2x_3\frac{x_{12}^2}{x_{13}^2x_{23}^2}\left\{1+\bar{\alpha}_S b\left(\ln x_{12}^2\mu^2-\frac{x_{13}^2-x_{23}^2}{x_{12}^2}\ln\frac{x_{13}^2}{x_{23}^2}\right)+\bar{\alpha}_S\left(\frac{67}{36}-\frac{\pi^2}{12}-\frac{5}{18}\frac{N_f}{N_c}-\frac{1}{2}\ln\frac{x_{13}^2}{x_{12}^2}\ln\frac{x_{23}^2}{x_{12}^2}\right)\right\}S_{12} \quad (16)$$

where $S_{12}\equiv 1-N(x_{12},b,Y)$.

The integral over x_3 is taken in Appendix B and Eq. (16) can be written in the form

$$\frac{\mathrm{d}\ln S_{12}}{\mathrm{d}Y} = -\bar{\alpha}_S\left[1+\bar{\alpha}_S b\ln(\mu^2 x_{12}^2)+\bar{\alpha}_S\left(\frac{67}{36}-\frac{\pi^2}{12}-\frac{5}{18}\frac{N_f}{N_c}\right)\right]\ln(Q_s^2x_{12}^2)+\frac{\bar{\alpha}_S^2 b}{2}\ln^2 Q_s^2x_{12}^2+\bar{\alpha}_S\zeta(3). \tag{17}$$

In Eq. (17) almost all terms are functions of $z=\ln(x_{12}^2Q_s^2)$, except the term $\bar{\alpha}_S b\ln(\mu^2x_{12}^2)\ln(Q_s^2x_{12}^2)$. Introducing the new renormalization point Q_s^2 instead of μ^2 the equations reduce to the following one:

$$\frac{\mathrm{d}\ln S_{12}}{\mathrm{d}Y} = -\bar{\alpha}_S(Q_s)\left[1+\frac{1}{2}\bar{\alpha}_S(Q_s)b\ln(Q_s^2x_{12}^2)+\bar{\alpha}_S(Q_s)\left(\frac{67}{36}-\frac{\pi^2}{12}-\frac{5}{18}\frac{N_f}{N_c}\right)\right]\ln(Q_s^2x_{12}^2)+\bar{\alpha}_S(Q_s)\zeta(3). \tag{18}$$

Introducing a new variable

$$z=\ln(Q_s^2x_{12}^2)=\bar{\alpha}_S(Q_s)\varrho(Y-Y_0)+\ln(x_{12}^2Q_0^2)\overset{Y-Y_0\gg1}{\longrightarrow}\bar{\alpha}_S(Q_s)\lambda(\gamma_{cr})(Y-Y_0)+\ln(x_{12}^2Q_0^2) \tag{19}$$

and replacing $\partial/\partial Y$ by $(1/\rho)d/dz$, Eq. (18) takes the form

$$\frac{\mathrm{d}\ln S_{12}}{\mathrm{d}z} = -\frac{1}{\varrho}\left(\left[1+\frac{1}{2}\bar{\alpha}_S(Q_s)bz+\bar{\alpha}_S(Q_s)\left(\frac{67}{36}-\frac{\pi^2}{12}-\frac{5}{18}\frac{N_f}{N_c}\right)\right]z+\zeta(3)\right). \tag{20}$$

Integration over z leads to

$$\ln S_{12} = -\frac{1}{2\varrho}\left(\left[z+\frac{1}{3}\bar{\alpha}_S(Q_s)bz^2+\bar{\alpha}_S(Q_s)z\left(\frac{67}{36}-\frac{\pi^2}{12}-5\frac{N_f}{N_c}\right)\right]z+2\zeta(3)z\right). \tag{21}$$

Finally,

$$1-N(z)=e^{-\mathcal{Z}(z;Q_s)}\quad\text{with}\quad\mathcal{Z}(z;Q_s)=\frac{1}{2\varrho}\left(\left[z+\frac{1}{3}\bar{\alpha}_S(Q_s)bz^2+\bar{\alpha}_S(Q_s)z\left(\frac{67}{36}-\frac{\pi^2}{12}-\frac{5}{18}\frac{N_f}{N_c}\right)\right]z+2\zeta(3)z\right). \tag{22}$$

The main term in Eq. (22) has the form $z^2/(2\lambda(\gamma_{cr}))$, and displays geometric scaling behavior. We would like to stress, that such behavior occurs only, if we assume that the renormalization scale $\mu=Q_s$. Generally, Eq. (22) leads to the violations of the geometric scale in the NLO, which are proportional to $\bar{\alpha}_S(Q_s)z$. Equation (22) shows, for the first time, that the intuitive expectation, that the only scale inside of the saturation region is the saturation momentum, holds at least in the NLO. On the other hand, we can interpret Eq. (22), as a new geometric scaling behavior for the amplitude, which turns out to be dependent on the variable $\mathcal{Z}(z;Q_s)$.

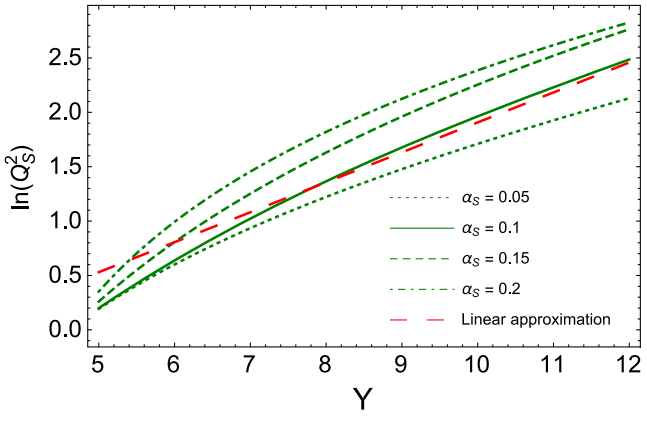

FIG. 4. $\ln(Q_s(b,Y)/Q_s(b,Y=Y_0))$ versus Y at different values of $\bar{\alpha}_S$. $Y_0=4.6$. For the linear approximation we plot $0.7\lambda_{cr}(Y-Y_0)$ at $\bar{\alpha}_S=0.1$.

E. Matching at $r^2Q^2(b,Y)=1$

In Sec. II C we saw that the amplitude in the vicinity of the saturation scale has a geometric scaling behavior [see Eq. (13)] as well as the amplitude at $r^2Q_s^2\gg1$, as has been shown in the previous section. The first observation is that we can match these two amplitudes, only if we assume that the renormalization scale $\mu=Q_s$. Practically, it means that we have to replace $\bar{\alpha}_S$ in Sec. II C with $\bar{\alpha}_S(Q_s)$. This generates an additional Y dependence, diminishing the value of λ_{cr} at large values of Y.

The general matching conditions (see Fig. 5) have the form of the two following equations at $z=z_m$: we match these two solution at $z=z_m$ where

$$N^{0<z\ll 1}(z=z_m)=N^{z\gg 1}(z=z_m),$$
$$\frac{dN^{0<z\ll 1}(z=z_m)}{dz_m}=\frac{dN^{z\gg 1}(z=z_m)}{dz_m}. \tag{23}$$

These two equations determine the value of the amplitude and the point of matching. The additional restriction is that $z_m \ll 1$, or, in other words z_m should be in the vicinity of the saturation scale. A problem is that it is impossible to satisfy Eq. (23) without modifying the solution of Eq. (22). Most models in the past followed the suggestion of Ref. [14] and instead of Eq. (22), the modified solution

$$1-N(z)=e^{-C\mathcal{Z}(z)} \tag{24}$$

was introduced, in which the value of the constant C was determined by the matching conditions of Eq. (23). In Ref. [38] the correction to the asymptotic solution of Eq. (22) was found, which allows us to use the solution of Eq. (22) without an arbitrary unjustified constant C. This solution takes the form

$$N^{z\gg 1}(z)=1-2Ae^{-\mathcal{Z}}-A^2\frac{1}{\mathcal{Z}}e^{-2\mathcal{Z}}+\mathcal{O}(e^{-3\mathcal{Z}})$$
$$\mathcal{Z}=\mathcal{Z}\left(Eq.\ (22), z\to z-\frac{1}{2}A\sqrt{\varrho\pi/2}-2\psi(1)\right) \tag{25}$$

where $\psi(x)$ is the digamma function (see Ref. [45] Eqs. 8.360–8.367).

The second term in Eq. (25) is the solution given in Ref. [33], in which the theoretically unknown constant A was introduced, both as the coefficient in front, and as the correction to the argument. The third term is the next-order correction at large z. In Refs. [1,38] it has been demonstrated that using Eq. (25), we can solve Eq. (23) and find z_m (see Fig. 5).

F. Impact parameter dependence of the saturation scale

So far we have introduced only one phenomenological parameter N_0, the value of the scattering amplitude at $r^2Q_s^2=1$. However, we need to specify the value of the saturation scale at $Y=Y_0$. It includes the value of the saturation scale and its dependence on the impact parameter b. Both can only be estimated in nonperturbative QCD. Due to the embryonic stage of our understanding of the nonperturbative QCD contribution, we can only suggest a phenomenological parametrization.

For $Q_s(Y=Y_0,b)$ we use the following expression:

$$Q_s^2(Y=Y_0,b)=Q_0^2S(b)=Q_0^2(mbK_1(mb))^{1/(1-\gamma_{cr})}. \tag{26}$$

The value of m has to be found from the fitting of the experimental data. We expect that $m\approx 0.5\div 0.85$ GeV since $m=0.72$ GeV is the scale for the electromagnetic form factor of the proton, while $m\approx 0.5$ GeV is the scale for the so-called gluon mass [46].

We differ from other models in that Eq. (26) leads to $Q_s^2(Y=Y_0,b)\overset{mb\gg 1}{\to}\exp(-mb/(1-\gamma_{cr}))$, providing the correct large-b behavior of the scattering amplitude. It should be stressed that the exponential decrease at large b, follows from a general theoretical approach, based on analyticity and unitarity of the scattering amplitude (see Ref. [8]). Therefore, $Q_s^2(Y=Y_0,b)\propto\exp(-b^2/B)$ that was used in other models (see Refs. [17–21,24,29]) are in direct contradiction with theory. The behavior of the amplitude at large b determines the energy dependence of the interaction radius, leading to $R\propto(1/m)Y$ for the exponential decrease, and $R\propto(1/m)\sqrt{Y}$ for the Gaussian b dependence. Such a difference, leads to a fast increase of the scattering amplitude for our parametrization and it will affect the predictions at high energy.

Equation (26) gives the amplitude in the vicinity of the saturation scale, which is proportional to $S(b)$ and generates the behavior $1/(1+\frac{Q_T^2}{m^2})^2$, where Q_T is the momentum transfer. At large Q_T the amplitude in our parametrization is proportional ($A\propto 1/Q_T^4$) as it follows from the perturbative QCD calculation [9], but cannot be reproduced with the Gaussian distribution.

G. Wave functions

The wave function in the master equation [see Eq. (2)] is the main source of theoretical uncertainties: even in the case of deep inelastic processes, we can trust the wave function of perturbative QCD only, at rather large values of $Q^2\geq Q_0^2$ with $Q_0^2\approx 0.7$ GeV^2 (see Ref. [47]). The expression for $(\Psi^*\Psi)^{\gamma^*}\equiv\Psi_{\gamma^*}(Q,r,z)\Psi_{\gamma^*}(Q,r,z)$ is well known (see Ref. [2] and references therein)

$$(\Psi^*\Psi)_T^{\gamma^*}=\frac{2N_c}{\pi}\alpha_{\rm em}\sum_f e_f^2\{[z^2+(1-z)^2]\epsilon^2K_1^2(\epsilon r)+m_f^2K_0^2(\epsilon r)\}, \tag{27}$$

$$(\Psi^*\Psi)_L^{\gamma^*}=\frac{8N_c}{\pi}\alpha_{\rm em}\sum_f e_f^2Q^2z^2(1-z)^2K_0^2(\epsilon r), \tag{28}$$

where T (L) denotes the polarization of the photon and f represents the flavors of the quarks. $\epsilon^2=m_f^2+Q^2z(1-z)$.

TABLE I. Parameters of the model. $\bar{\alpha}_{S0}$, N_0, m and Q_0^2 are fitted parameters. The masses of quarks are chosen as they are shown in the table. Two sets are related to two choices of the quark masses: the current masses and the masses of light quarks are equal to 140 MeV which is the typical infrared cutoff in our approach.

$\bar{\alpha}_{S0}$	N_0	Y_0	m(GeV)	Q_0^2(GeV^2)	m_u(MeV)	m_d(MeV)	m_s(MeV)	m_c(GeV)	χ^2/d.o.f.
0.133	0.1075	3.77	0.83	3.0	2.3	4.8	95	1.4	$183/153 = 1.2$
0.143	0.0915	3.73	0.67	2.6	140	140	140	1.4	$242/153 = 1.58$
0.133	0.107	3.77	0.828	2.93	2.3	4.8	95	1.27	$193.31/153 = 1.26$

III. FITTING F_2 AND VALUES OF THE PARAMETERS

The most accurate experimental data available are for the deep inelastic structure function F_2 [48], which we will attempt to fit using the model. As has been mentioned, we can trust our model in the restricted kinematic region, which we choose in the following way: 0.85 GeV$^2 \leq Q^2 \leq$ 60 GeV^2 and $x \leq 0.01$. The lower limit of Q^2 stems from the nonperturbative correction to the wave function of the virtual photon, while the upper limit originates from the restriction $x \leq 0.01$. This restriction can be translated to the value of Y_0 in our theoretical formulas leading to $Y_0 = 4.6$. Actually we view Y_0 as the parameter of the fit (see Table I).

The energy dependence of the saturation scale Q_s and the $\tau = r^2 Q_s^2(b, Y)$ dependence of the scattering amplitude are determined by Eq. (11) and Eq. (23). One can see that both depend on $\bar{\alpha}_S(Q_s)$ for which we use Eq. (12). From this equation one can see that we have two fitting parameters: $\bar{\alpha}_{S0}$ and Q_0^2. In principle, $\bar{\alpha}_{S0}$ is the running QCD coupling at $Q^2 = Q_0^2$, but we consider both $\bar{\alpha}_{S0}$ and Q_0^2 as independent fitting parameters, since we do not want to fix the value of $\Lambda_{\rm QCD}$. We have two dimensional parameters: Q_0, which determines the value of Q_s^2, and m which determines its dependence on impact parameters b (see Sec. II F). N_0 is the value of the scattering amplitude at $\tau = 1$. In principle, the value of N_0 can be calculated using the linear evolution equation with the initial conditions. However, it depends on the phenomenological parameters of this initial condition. So we choose N_0 as a fitting parameter.

It is worth mentioning that $\lambda_{cr}, \gamma_{cr}$ are not the fitting parameters as they are in the leading-order models. We recall that

$$\ln\left(Q_s^2(b, Y)/Q_s^2(b, Y = Y_0)\right) = d_0(\bar{\alpha}_S)Y + d_1(\bar{\alpha}_S)\ln\left(Y/Y_0\right) - d_2(\bar{\alpha}_S)\left(\frac{1}{\sqrt{Y}} - \frac{1}{\sqrt{Y_0}}\right) \tag{29}$$

where the functions d_i are shown in Fig. 6. In Eq. (29) $Y = \ln(1/x)$, where x is the Bjorken $x = Q^2/s$ for the deep inelastic scattering with the light quarks (Q is the photon virtuality and s is the energy squared of collision). For the charm quark we consider $Y_c = \ln(1/x_c)$ with $x_c = (1 + 4m_c^2/Q^2)x$.

We do not regard the masses of the quarks as fitting parameters and consider two sets of these masses. In the first set we take the current masses (see the first row of Table I), and we consider this as the most reliable fit, based on the consistent theoretical approach. It should be mentioned that for the description of the interaction with the c quark we use $Y = \ln(1/x_c)$ with $x_c = x/(1 + 4m_c^2/Q^2)$. In Table I we take two values of the m_c mass: $m_c = 1.4$ GeV and $m_c = 1.27$ GeV. We see that two sets of parameters differ comparatively little with a small preference for

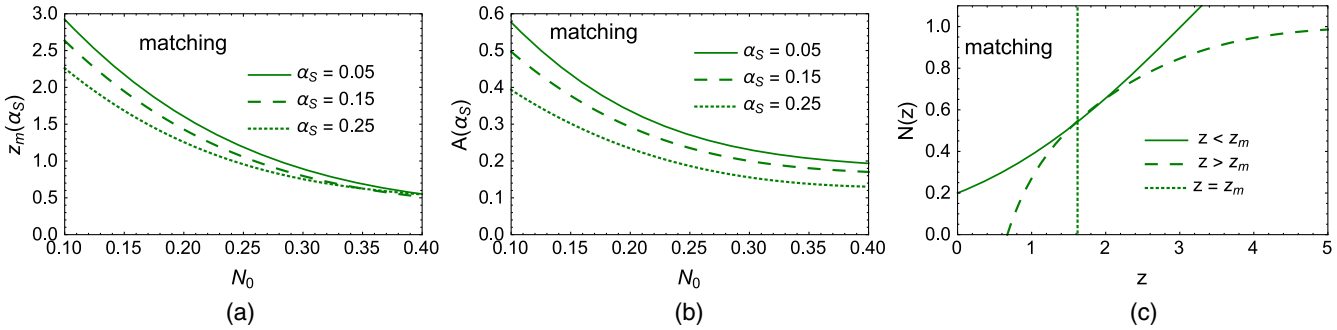

FIG. 5. Matching procedure: the function $z_m(N_0, \bar{\alpha}_S)$ (a), the function $A(N_0, \bar{\alpha}_S)$ (b) and the example of the resulting function for $N_0 = 0.1$ and $\bar{\alpha}_S = 0.15$ (c).

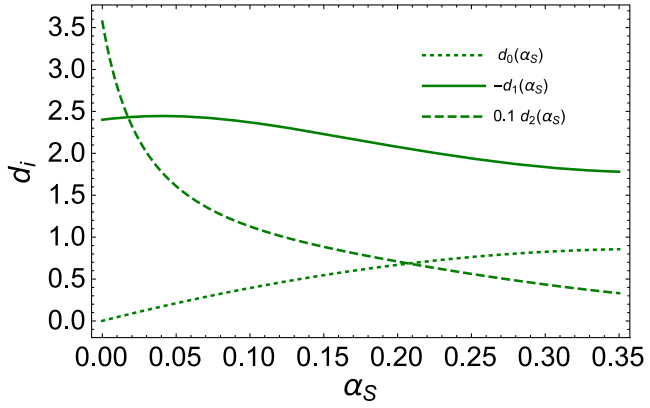

FIG. 6. The functions $d_i(\bar{\alpha}_S)$ of Eq. (29) versus $\bar{\alpha}_S$.

$m_c = 1.4$ GeV which leads to $\chi^2/\text{d.o.f.} = 1.2$ while $\chi^2/\text{d.o.f.} = 1.26$ for $m_c = 1.27$ GeV.

We also make a fit putting all masses of light quarks (second row of Table I) to be equal to 140 MeV. We view this mass as a typical infrared cutoff that we introduce to take into account the unknown mechanism of confinement.

Table I gives the values of the fitting parameters, and Fig. 7 demonstrates the quality of the fit. One can see that we describe the data quite well but we have to admit that the quality of the fit is worse than in our model based on leading-order QCD estimates [1], in which we fitted the

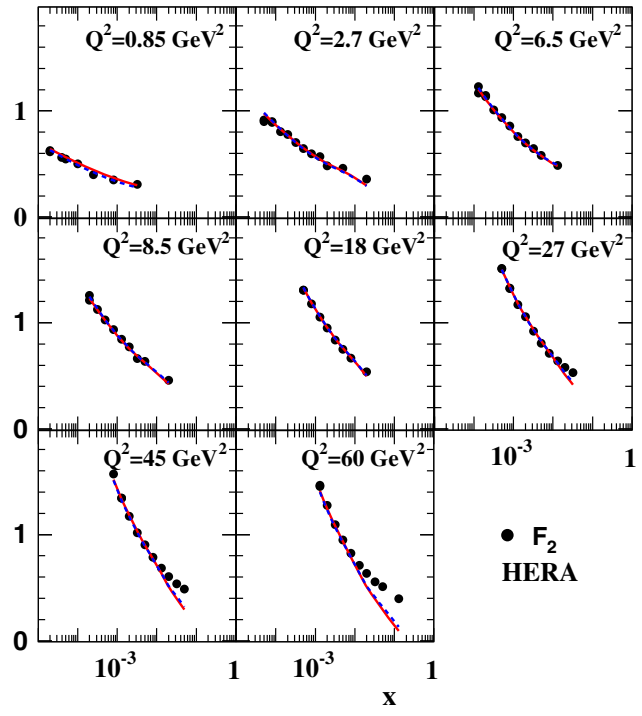

FIG. 7. Our fit of F_2 with the values of the parameters given in Table I. The first set of parameters is shown as solid red curves while the second is shown as blue dotted lines. The data are taken from Ref. [48].

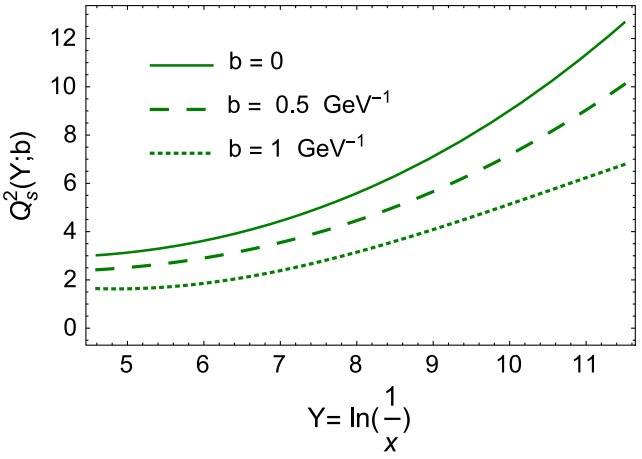

FIG. 8. The value of the saturation momentum $Q_s^2(x,b)$ versus x at fixed b for the parameters given by Table I.

value of λ_{cr}. $\chi^2/\text{d.o.f.} = 1.3$ in this fit against $\chi^2/\text{d.o.f.} = 1.15$ in the fit of Ref. [1]. However, the main complication of this model is that it gives a rather large value of Q_0^2 (see Fig. 8) which is in sharp contradiction to the value of the saturation momentum, from all other model descriptions of the experimental data [1,10–29]. The large value of Q_0^2 is in agreement with small values of $\bar{\alpha}_{S0}$, and we note that $\bar{\alpha}_{S0} = 0.28$ for $\Lambda_{\text{QCD}} = 158$ MeV instead of $\bar{\alpha}_{S0} = 0.13$ from our fit.

The value of m is larger than the typical mass in the electromagnetic form factor of the proton, but we do not expect it to be the same. Note that the decrease of Q_s^2 at large b is proportional to $\exp\left(-\frac{m}{1-\gamma_{cr}}b\right) = \exp\left(-1.6(\text{GeV}^{-1})b\right)$. On the other hand the behavior of the amplitude with respect to b differs from the saturation scale. In Fig. 9 one can see that both the saturation, and the violation of the geometric scaling behavior influence the resulting b dependence of the scattering amplitude. Saturation flattens the b dependence at small values of b, while the large-b behavior shows a more rapid decrease than the b dependence of the saturation scale (see Fig. 9).

It should be stressed that in the framework of our parametrization of the b dependence of the saturation momentum, the scattering amplitude decreases as

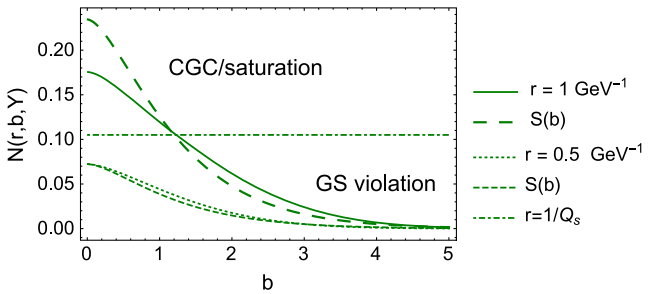

FIG. 9. The b-dependence of the scattering amplitude for the parameters given by Table I. $S(b)$ is given by Eq. (1).

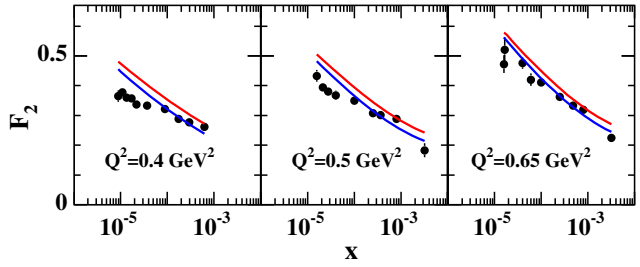

FIG. 10. The x dependence of $F_2^{c\bar{c}}$ at small values of $Q^2 < 0.85$ GeV^2 for the parameters given in Table I. The red (upper) line corresponds to set 1 (upper row of Table I) while the blue (lower) one is the description with set 2. The data are taken from Refs. [49,50].

$\exp(-mb)$ while in all other models on the market it has a Gaussian behavior: $\exp(-m^2b^2)$.

In. Fig. 10 we present the comparison between our fit of F_2 with two sets of parameters at low values of Q. The set with large masses of quarks leads to a much better description illustrating that the nonperturbative corrections to the wave function of the virtual photon are essential at $Q^2 < 0.85$ GeV^2. To illustrate the influence of the bad description of the data at $Q^2 < 0.85$ GeV^2 we include in the fit the data at $Q^2 = 0.5$ GeV^2 and at $Q^2 = 0.4$ GeV^2. The set of fitting parameters remains the same but χ^2/d.o.f. increases more than 3 times.

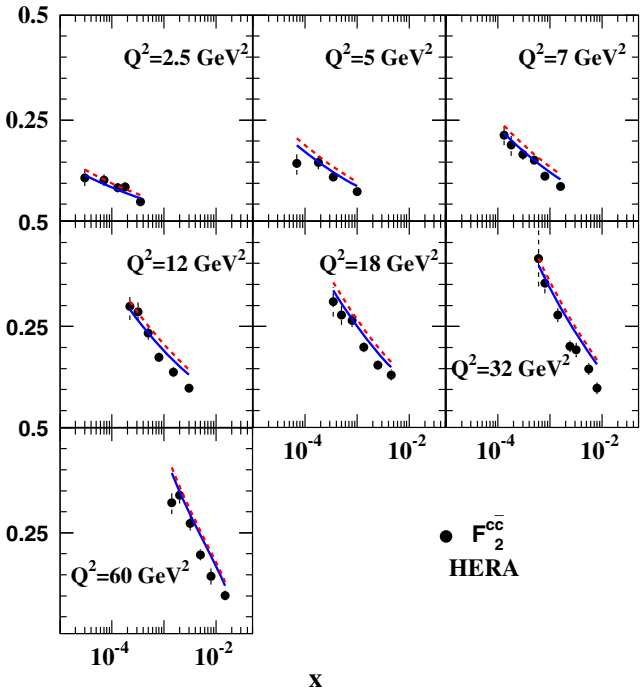

FIG. 11. The x dependence of $F_2^{c\bar{c}}$ at fixed values of Q^2: $0.85 \leq Q^2 \leq 60$ GeV^2 for the parameters given in Table I: the solid lines correspond $m_c = 1.4$ GeV while the dashed ones describe the data for $m_c = 1.27$ GeV. The data are taken from Ref. [51].

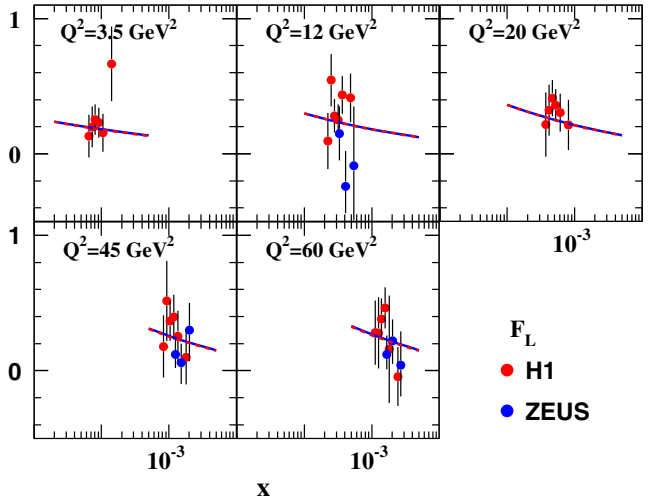

FIG. 12. The x dependence of F_L at fixed values of Q^2: $0.85 \leq Q^2 \leq 60$ GeV^2 for the parameters given in Table I. The red (blue) lines correspond to set 1 (set 2) fits. The data are taken from Ref. [50].

$F_2^{c\bar{c}}$: The contribution of the $c\bar{c}$ pair to the deep inelastic structure function can be calculated with the same theoretical accuracy as the inclusive F_2. In Fig. 11 we compare the HERA data on F_2^{cc} [51] with the theoretical predictions. One can see that the agreement is reasonable. The difference in mass of the c quark does not affect the comparison with the experimental data (see solid sand dashed lines in Fig. 11).

F_L: F_L can be calculated to the same accuracy as $F_2^{c\bar{c}}$, and the comparison with the scant data available [49,50] is plotted in Fig. 12. The two sets produce the same quality of the descriptions since the values of Q are rather large.

In Ref. [1] we compared the model with data on exclusive production in deep inelastic scattering (DIS). The most interesting information, from these processes, concerns the momentum transfer (t) dependence of the differential cross sections, which could check the novel ingredient of our model: the exponential dependence of the scattering amplitude on the impact parameter. In Ref. [1] it was shown that, this dependence agrees with the experimental data. In the present approach the b dependence is taken the same as in Ref. [1]. Hence we can only check the slight difference in the values of the typical mass (see Table II). This difference leads to the slight ($\leq$10%) change of the t slope for the differential cross section. Unfortunately, the experimental accuracy of the slope measurement is larger than this expected change (see Figs. 11 and 12 of Ref. [1]). Therefore, we are of the opinion, that the comparison with the exclusive cross section, cannot teach us anything, and we decided not to make a comparison with these measurements at present.

TABLE II. Fitted parameters of the model.

$\lambda(\lambda_{\rm eff})$	N_0	m(GeV)	Q_0^2(GeV^2)	m_u(MeV)	m_d(MeV)	m_s(MeV)	m_c(GeV)	χ^2/d.o.f.	Model
0.197	0.34	0.75	0.145	2.3	4.8	95	1.4	1.15	LO
0.5(0.35)	0.1075	0.83	3.0	2.3	4.8	95	1.4	1.2	NLO
0.184	0.46	0.75	0.118	140	140	140	1.4	1.14	LO
0.53(0.37)	0.09	0.67	2.6	140	140	140	1.4	1.58	NLO

IV. CONCLUSIONS

In this paper we made the first attempt to include everything, that we have learned about the next-to-leading corrections of perturbative QCD, in the CGC/saturation model. In this paper we obtained two new theoretical results: using the approach suggested in Ref. [33], we obtained (i) the asymptotic behavior of the solution to the Balitsky-Kovchegov equation in the NLO of perturbative QCD [30–32] deep inside the saturation domain, and (ii) the approximate geometric scaling behavior of the scattering amplitude, which holds in the leading term at large z ($\propto z^2$) only if $\tau = r^2 Q_s^2(Y;b)$ is determined in perturbative QCD with the renormalization scale $Q_s(Y;b)$ and which is violated by $\bar{\alpha}_S(Q_s)z$ terms. As far as we can establish, this is the first theoretical justification, for the intuitive suggestion from LO estimates, that the entire behavior of the scattering amplitude in the saturation domain, is determined by the only dimensional observable: the saturation scale. We can also interpret our result, given by Eq. (22), as the new scaling behavior for the scattering amplitude, which turns out to be dependent on the variable $\mathcal{Z}(z;Q_s)$.

In the model we included several known ingredients: (i) the behavior of the scattering amplitude in the vicinity of the saturation momentum, using the NLO BFKL kernel, (ii) the pre-asymptotic behavior of $\ln(Q_s^2(Y))$ as a function of Y and (iii) the impact parameter behavior of the saturation momentum which has exponential behavior $\propto \exp(-mb)$ at large b.

In comparison with the models on the market [10–29], we added the NLO corrections both deep in the saturation domain and in the vicinity of the saturation scale, as well as two crucial ingredients following Ref. [1]: the correct solution to the nonlinear (BK) equation [6] in the saturation region, and the impact parameter distribution that leads to an exponential decrease of the saturation momentum at large impact parameters and to a power-like decrease at large transfer momentum that follows from perturbative QCD [9].

In spite of the fact that we described the experimental data fairly we are aware that our description is worse than in the CGC/saturation models based on the leading-order QCD approach. The main difficulties are related to the small value of the QCD coupling at $Q_s(Y_0)$, and the large values of the saturation momentum, which show the theoretical inconsistency of our description. To see our difficulties more distinctly, we compare the results of the fits with our LO model [1] shown in Table II. One can see that in spite of a good description of the experimental data, with reasonable $\chi^2_{\rm d.o.f.}$, the energy behavior [the values of $\lambda(\lambda_{eft})$] and the value of Q_0 turn out to be different. These two parameters lead to the large values of the saturation scale which is in a qualitative agreement with the small values of $\bar{\alpha}_S$ (see Table I). However, we need to assume a very small $\Lambda_{\rm QCD} \sim 10$ MeV to obtain $\bar{\alpha}_{S0} \approx 0.13 - 0.16$ which results from the fit (see Table I).

Nevertheless, we could view the result of our fit differently, stating that the DIS data demands large values of the saturation momentum. In this case, we need to change the strategy of fitting using the reduced cross sections (σ_r) instead of F_2[2] which have been used. Indeed, σ_r is not influenced by any theoretical assumption on the extraction of the structure functions. As we have a sceptical view of the result of our fit, we prefer to use F_2, which we used in our previous attempt to fit DIS data [1,52], to compare the results of different approaches.

Appreciating the difficulties of our approach, we need to improve our theoretical input. We cannot avoid the main assumption that the nonperturbative b dependence is absorbed in the impact parameter behavior of the saturation scale. However we are planning to improve the matching procedure given by Eq. (23), assuming the geometric scaling behavior of the scattering amplitude as it stems from the form of the z dependence at large z of the scattering amplitude found in this paper. We are also investigating the possibility to go beyond the NLO approximation. As we have discussed, for the scattering amplitude in the vicinity of the saturation scale we used Salam resummation [40], which is the technique to take the particular corrections beyond NLO. We need to find a method to expand this resummation to the entire saturation region.

In future attempts to improve our model, we believe that another approach based on the BK equation beyond the LO [53], will be very instructive. In Ref. [53] the generalization of the BK equation which sums part of the NLO effects, which are enhanced by large transverse logs, that have been summed to all orders, was proposed. The advantage of this approach provides a possibility to treat large z on a theoretical basis, without matching. However, there are two problems, which make this approach dubious: (i) the double log approximation and its modification cannot contribute to the scattering amplitude deep in the saturation

[2]We thank our referee for drawing our attention to this strategy.

region,[3] and the Salam resuming [40] of all order corrections in the vicinity of the saturation momentum leads to quite different values for λ (see Table II) than has been estimated in Ref. [53]. Note, that this approach describes DIS data quite well, and no worse than our approach, or the approaches of the models of Refs. [10–29] demonstrating the fact, that the experimental data alone, cannot differentiate between theoretically correct and theoretically insufficient, (or even wrong) approaches.

ACKNOWLEDGMENTS

We thank our colleagues at Tel Aviv university and UTFSM for encouraging discussions. Our special thanks go to Asher Gotsman, Alex Kovner and Misha Lublinsky for elucidating discussions on the subject of this paper. This research was supported by the BSF Grant No. 2012124, by Proyecto Basal FB 0821(Chile), Fondecyt (Chile) Grants No. 1130549 and 1140842, CONICYT Grant No. PIA ACT1406 and by DGIP/USM Grant No. 11.15.41.

APPENDIX A: RESUMED KERNEL OF THE NLO BFKL EQUATION

For completeness of presentation we collect in this appendix all formulas for the NLO kernel of the BFKL equation, [39] resumed according to the procedure, suggested in Ref. [40].

$$\chi^{\rm NLO}(f) = -\frac{1}{4}\Big(2b(\chi'(f)+\chi(f)^2)+\chi''(f) - \Big(\frac{67}{9}-\frac{\pi^2}{3}-\frac{10}{9}\Big)\chi(f) \tag{A1}$$

$$+\frac{\pi^2\cos(\pi f)\left(\frac{(3f(1-f)+2)\left(\frac{N_f}{N_c^3}+1\right)}{(3-2f)(2f+1)}+3\right)}{(1-2f)\sin^2(\pi f)}+4\phi(f) -\frac{\pi^3}{\sin(\pi f)}-6\zeta(3)\Big)-\frac{1}{2}\chi(f)\chi'(f)+\frac{\chi(f)}{(1-f)^2}, \tag{A2}$$

$$\phi(f)=\sum_{n=1}^{\infty}(-1)^n\Big(\frac{\psi(-f+n+2)-\psi(1)}{(-f+n+1)^2} +\frac{\psi(f+n+1)-\psi(1)}{(f+n)^2}\Big), \tag{A3}$$

$$A_{GG}(\omega)=b-\frac{1}{\omega+1}+\frac{1}{\omega+2}-\frac{1}{\omega+3} -(\psi(\omega+2)-\psi(1)),$$
$$A_{QG}(\omega)=\frac{N_f}{N_c+2}\Big(-\frac{2}{\omega+2}+\frac{2}{\omega+3}+\frac{1}{\omega+1}\Big),$$
$$AA(\omega)=A_{GG}(\omega)+\frac{C_f}{N_c}A_{QG}(\omega), \tag{A4}$$

$$b=\frac{11N_c-2N_f}{12N_c},\qquad C_F=\frac{N_c^2-1}{2N_c},$$
$$F=\frac{N_f}{6N_c}\Big(\frac{5}{3}+\frac{13}{6N_c^2}\Big),$$
$$\bar\alpha_S(p^2)=\frac{1}{b\ln(p^2/\Lambda^2_{\rm QCD})} =\frac{\bar\alpha_S(\mu)}{1+b\bar\alpha_S(\mu)\ln(p^2/\mu^2)}. \tag{A5}$$

In Ref. [42] a very elegant form of $\chi_1(\omega,\gamma)$ was suggested which coincides with Eq. (6) to within 7%. The equation for ω takes the form

$$\omega=\bar\alpha_S(1-\omega)\Big(\frac{1}{f}+\frac{1}{1-f+\omega} +\underbrace{(2\psi(1)-\psi(2-f)-\psi(1+f))}_{\text{high twist contributions}}\Big). \tag{A6}$$

One can see that $\gamma(\omega)\to 0$ when $\omega\to 1$ as follows from energy conservation.

In Fig. 13 we plot the values of λ_{cr} and γ_{cr} for the full kernel of Eq. (6) and for the simplified kernel of Eq. (A6) suggested in Ref. [42]. One can see that in spite of the fact that the simplified kernel coincides with the full one to within 7%, the differences in λ_{cr} and in γ_{cr} are much larger.

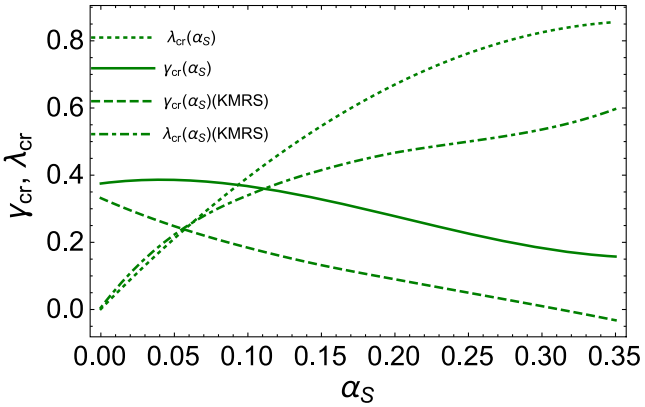

FIG. 13. $\lambda(\gamma_{cr})$ and γ_{cr} versus α_S for the full NLO kernel of Eq. (6) and for the kernel of Eq. (A6).

[3]See the thorough analysis of this statement in Ref. [42] and the small contribution of the double log term in our solution for the scattering amplitude deep in the saturation region. Comparing the I_3 term in Eq. (B3) and Eq. (B5) we see that the double log terms lead to the corrections of the order of z in $\mathcal{Z}$ of Eq. (22). We also recall that it has been shown in Ref. [33] that inside the saturation region the most important term in the BFKL kernel is not the double log term.

APPENDIX B: CALCULATION OF INTEGRALS FOR THE SOLUTION IN THE SATURATION REGION

In this appendix we take the integral of Eq. (16), which has the form

$$\frac{dS_{12}}{dY} = -\frac{\bar{\alpha}_S}{2\pi} K(Q_{s,} x_{12}) S_{12} \tag{B1}$$

where

$$K(Q_s, x_{12}) = \int d^2x_3 \frac{x_{12}^2}{x_{13}^2 x_{23}^2}\left[1 + \bar{\alpha}_S b\left(\ln(\mu^2 x_{12}^2) - \frac{x_{13}^2 - x_{23}^2}{x_{12}^2}\ln\frac{x_{13}^2}{x_{23}^2}\right) + \bar{\alpha}_S\left(\frac{67}{36} - \frac{\pi^2}{12} - \frac{5}{18}\frac{N_f}{N_c} - \frac{1}{2}\ln\frac{x_{13}^2}{x_{12}^2}\ln\frac{x_{23}^2}{x_{12}^2}\right)\right]. \tag{B2}$$

Introducing the notations

$$\begin{aligned} I_1 &= \int d^2x_3 \frac{x_{12}^2}{x_{13}^2 x_{23}^2}\left[1 + \bar{\alpha}_S b \ln(\mu^2 x_{12}^2) + \bar{\alpha}_S\left(\frac{67}{36} - \frac{\pi^2}{12} - \frac{5}{18}\frac{N_f}{N_c}\right)\right], \\ I_2 &= \bar{\alpha}_S b \int d^2x_3 \frac{x_{12}^2}{x_{13}^2 x_{23}^2}\left[\frac{x_{23}^2 - x_{13}^2}{x_{12}^2}\ln\left(\frac{x_{13}}{x_{23}}\right)\right], \\ I_3 &= -\frac{\bar{\alpha}_S}{2}\int d^2x_3 \frac{x_{12}^2}{x_{13}^2 x_{23}^2}\ln\frac{x_{13}^2}{x_{12}^2}\ln\frac{x_{23}^2}{x_{12}^2}, \end{aligned} \tag{B3}$$

we have

$$K(Q_s z_{12}) = I_1 + I_2 + I_3.$$

Using the symmetry of the integrand with respect to $x_{13} \leftrightarrow x_{32}$ we obtain

$$\begin{aligned} I_2 &= \alpha\beta \int d^2x_3 \frac{1}{x_{13}^2}\ln\left(\frac{x_{13}}{x_{23}}\right) - \bar{\alpha}_S b \int d^2x_3 \frac{1}{x_{23}^2}\ln\left(\frac{x_{13}}{x_{23}}\right) \\ &= \alpha\beta \int d^2x_3 \frac{1}{x_{13}^2}\ln\left(\frac{x_{13}}{x_{23}}\right) + \bar{\alpha}_S b \int d^2x_3 \frac{1}{x_{23}^2}\ln\left(\frac{x_{23}}{x_{13}}\right) \\ &= \alpha\beta \int d^2x_{13} \frac{1}{x_{13}^2}\ln\left(\frac{x_{13}}{x_{23}}\right) + \bar{\alpha}_S b \int d^2x_{23} \frac{1}{x_{23}^2}\ln\left(\frac{x_{23}}{x_{13}}\right) = 2\alpha\beta \int d^2x_{13} \frac{1}{x_{13}^2}\ln\left(\frac{x_{13}}{x_{23}}\right). \end{aligned} \tag{B4}$$

I_i in polar coordinates take the forms

$$\begin{aligned} I_1 &= \frac{1}{2}\int_{r_0^2}^{r_1^2}\frac{dr^2}{r^2}\int_0^{2\pi}\frac{1}{1 + r^2 - 2r\cos\theta}d\theta\left[1 + \bar{\alpha}_S b\ln(\mu^2 x_{12}^2) + \bar{\alpha}_S\left(\frac{67}{36} - \frac{\pi^2}{12} - \frac{5}{18}\frac{N_f}{N_c}\right)\right], \\ I_2 &= \bar{\alpha}_S b\int_{r_0^2}^{r_1^2}\frac{dr^2}{r^2}\int_0^{2\pi}\ln\left(\frac{r^2}{1 + r^2 - 2r\cos\theta}\right)d\theta, \\ I_3 &= -\frac{\bar{\alpha}_S}{4}\int_{r_0^2}^{r_1^2}\frac{dr^2}{r^2}\int_0^{2\pi}\frac{1}{1 + r^2 - 2r\cos\theta}\ln(r^2)\ln(1 + r^2 - 2r\cos\theta)d\theta \end{aligned} \tag{B5}$$

where $r^2 = x_{13}^2/x_{12}^2$, $r_0^2 = 1/Q_s^2 x_{12}^2$ and $r_1^2 = 1 - 1/Q_s^2 x_{12}^2$. We use the following representations to take the integral over the angle (see Ref. [45] Eqs. 1.448 and 1.511,3.613):

$$\begin{aligned} \int_0^{2\pi}\frac{\cos(n\theta)}{1 + r^2 - 2r\cos\theta}d\theta &= \frac{\Gamma(n+1)2\pi}{\Gamma(1)n!}r^n{}_2F_1(1, n+1; n+1, r^2) = 2\pi\frac{r^n}{1 - r^2}, \\ \ln(1 + r^2 - 2r\cos\theta) &= -2\sum_{n=1}^{\infty}\frac{\cos(n\theta)}{n}r^n, \qquad \ln(1 - r^2) = -\sum_{n=1}^{\infty}\frac{r^{2n}}{n}. \end{aligned} \tag{B6}$$

Using Eq. (B6) for $Q_s^2 x_{12}^2 \gg 1$ we obtain

$$
\begin{aligned}
I_1 &= \pi \int_{r_0^2}^{r_1^2} dr^2 \frac{1}{r^2(1-r^2)} \left[1 + \bar{\alpha}_S b \ln(\mu^2 x_{12}^2) + \bar{\alpha}_S \left(\frac{67}{36} - \frac{\pi^2}{12} - \frac{5}{18} \frac{N_f}{N_c} \right) \right] \\
&= 2\pi \left[1 + \bar{\alpha}_S b \ln(\mu^2 x_{12}^2) + \bar{\alpha}_S \left(\frac{67}{36} - \frac{\pi^2}{12} - \frac{5}{18} \frac{N_f}{N_c} \right) \right] \ln(Q_s^2 x_{12}^2), \\
I_2 &= 2\pi \bar{\alpha}_S b \int_{r_0^2}^{r_1^2} dr^2 \frac{\ln r^2}{r^2} d\theta = -\pi \bar{\alpha}_S b \ln^2 Q_s^2 x_{12}^2, \\
I_3 &= -\frac{\bar{\alpha}_S}{4} \int_{r_0^2}^{r_1^2} dr^2 \frac{\ln(r^2)}{r^2} \int_0^{2\pi} \frac{1}{1 + r^2 - 2r\cos\theta} \ln(1 + r^2 - 2r\cos\theta) d\theta \\
&= -\frac{\bar{\alpha}_S}{4} \int_{r_0^2}^{r_1^2} dr^2 \frac{\ln(r^2)}{r^2} (-2) \sum_{n=1}^{\infty} \frac{r^n}{n} \int_0^{2\pi} \frac{\cos\theta}{1 + r^2 - 2r\cos\theta} d\theta \\
&= -\frac{\bar{\alpha}_S}{4} \int_{r_0^2}^{r_1^2} dr^2 \frac{\ln(r^2)}{r^2} (-2) \sum_{n=1}^{\infty} \frac{r^n}{n} \left(\frac{2\pi r^n}{1 - r^2} \right) d\theta \\
&= -\frac{2\pi \bar{\alpha}_S}{2} \int_{r_0^2}^{r_1^2} dr^2 \frac{\ln(r^2) \ln(1 - r^2)}{r^2(1 - r^2)} d\theta = -2\pi \zeta(3).
\end{aligned} \tag{B7}
$$

Hence, we obtain the expression

$$
-\frac{\bar{\alpha}_S}{2\pi} K(Q_s z_{12}) = -\bar{\alpha}_S \left[1 + \bar{\alpha}_S b \ln(\mu^2 z_{12}^2) + \bar{\alpha}_S \left(\frac{67}{36} - \frac{\pi^2}{12} - \frac{5}{18} \frac{N_f}{N_c} \right) \right] \ln(Q_s^2 z_{12}^2) + \frac{\bar{\alpha}_S^2 b}{2} \ln^2 Q_s^2 z_{12}^2 + \bar{\alpha}_S \zeta(3) \tag{B8}
$$

which we have used in Sec. II D.

[1] C. Contreras, E. Levin, and I. Potashnikova, Nucl. Phys. **A948**, 1 (2016).

[2] Y. V. Kovchegov and E. Levin, *Quantum Chromodynamics at High Energies* (Cambridge University Press, Cambridge, England, 2012).

[3] A. Kovner and U. A. Wiedemann, Phys. Rev. D **66**, 051502 (2002); **66**, 034031 (2002); Phys. Lett. B **551**, 311 (2003).

[4] E. Ferreiro, E. Iancu, K. Itakura, and L. McLerran, Nucl. Phys. **A710**, 373 (2002).

[5] J. Jalilian-Marian, A. Kovner, A. Leonidov, and H. Weigert, Phys. Rev. D **59**, 014014 (1998); Nucl. Phys. **B504**, 415 (1997); J. Jalilian-Marian, A. Kovner, and H. Weigert, Phys. Rev. D **59**, 014015 (1998); A. Kovner, J. G. Milhano, and H. Weigert, Phys. Rev. D **62**, 114005 (2000); E. Iancu, A. Leonidov, and L. D. McLerran, Phys. Lett. B **510**, 133 (2001); Nucl. Phys. **A692**, 583 (2001); E. Ferreiro, E. Iancu, A. Leonidov, and L. McLerran, Nucl. Phys. **A703**, 489 (2002); H. Weigert, Nucl. Phys. **A703**, 823 (2002).

[6] I. Balitsky, Nucl. Phys. **B463**, 99 (1996); Phys. Rev. D **60**, 014020 (1999); Y. V. Kovchegov, Phys. Rev. D **60**, 034008 (1999).

[7] A. Kormilitzin, E. Levin, and S. Tapia, Nucl. Phys. **A872**, 245 (2011).

[8] M. Froissart, Phys. Rev. **123**, 1053 (1961); A. Martin, *Scattering Theory: Unitarity, Analitysity and Crossing* (Springer-Verlag, Berlin, 1969).

[9] G. P. Lepage and S. J. Brodsky, Phys. Rev. Lett. **43**, 545 (1979); Phys. Rev. Lett. **43**, 1625 (1979).

[10] K. J. Golec-Biernat and M. Wusthoff, Phys. Rev. D **60**, 114023 (1999); **59**, 014017 (1998).

[11] J. Bartels, K. J. Golec-Biernat, and H. Kowalski, Phys. Rev. D **66**, 014001 (2002).

[12] S. Bondarenko, M. Kozlov, and E. Levin, Nucl. Phys. **A727**, 139 (2003).

[13] H. Kowalski and D. Teaney, Phys. Rev. D **68**, 114005 (2003).

[14] E. Iancu, K. Itakura, and S. Munier, Phys. Lett. B **590**, 199 (2004).

[15] H. Kowalski, L. Motyka, and G. Watt, Phys. Rev. D **74**, 074016 (2006).

[16] H. Kowalski, T. Lappi, and R. Venugopalan, Phys. Rev. Lett. **100**, 022303 (2008).

[17] H. Kowalski, T. Lappi, C. Marquet, and R. Venugopalan, Phys. Rev. C **78**, 045201 (2008).

[18] G. Watt and H. Kowalski, Phys. Rev. D **78**, 014016 (2008).

[19] E. Levin and A. H. Rezaeian, Phys. Rev. D **82**, 014022 (2010).
[20] A. H. Rezaeian, Phys. Lett. B **718**, 1058 (2013).
[21] E. Levin and A. H. Rezaeian, Phys. Rev. D **83**, 114001 (2011).
[22] E. Levin and A. H. Rezaeian, Phys. Rev. D **82**, 054003 (2010).
[23] D. Boer *et al.*, arXiv:1108.1713.
[24] T. Lappi and H. Mantysaari, Phys. Rev. C **83**, 065202 (2011).
[25] T. Toll and T. Ullrich, Phys. Rev. C **87**, 024913 (2013).
[26] P. Tribedy and R. Venugopalan, Nucl. Phys. **A850**, 136 (2011); **A859**, 185(E) (2011).
[27] P. Tribedy and R. Venugopalan, Phys. Lett. B **710**, 125 (2012); **718**, 1154(E) (2013).
[28] A. H. Rezaeian, M. Siddikov, M. Van de Klundert, and R. Venugopalan, *Proc. Sci.*, DIS2013 (2013) 060, arXiv:1307.0165; Phys. Rev. D **87**, 034002 (2013).
[29] A. H. Rezaeian and I. Schmidt, Phys. Rev. D **88**, 074016 (2013).
[30] I. Balitsky, Phys. Rev. D **75**, 014001 (2007).
[31] Y. V. Kovchegov and H. Weigert, Nucl. Phys. **A784**, 188 (2007).
[32] I. Balitsky and G. A. Chirilli, Phys. Rev. D **77**, 014019 (2008); Nucl. Phys. **B822**, 45 (2009); Phys. Rev. D **88**, 111501 (2013).
[33] E. Levin and K. Tuchin, Nucl. Phys. **B573**, 833 (2000); **A691**, 779 (2001); **A693**, 787 (2001).
[34] J. Bartels and E. Levin, Nucl. Phys. **B387**, 617 (1992).
[35] A. M. Stasto, K. J. Golec-Biernat, and J. Kwiecinski, Phys. Rev. Lett. **86**, 596 (2001); L. McLerran and M. Praszalowicz, Acta Phys. Pol. B **42**, 99 (2011); **41**, 1917 (2010); M. Praszalowicz, Acta Phys. Pol. B **42**, 1557 (2011); M. Praszalowicz and T. Stebel, J. High Energy Phys. 03 (2013) 090; L. McLerran, M. Praszalowicz, and B. Schenke, Nucl. Phys. **A916**, 210 (2013); M. Praszalowicz, Phys. Lett. B **727**, 461 (2013); L. McLerran and M. Praszalowicz, Phys. Lett. B **741**, 246 (2015).
[36] E. Iancu, K. Itakura, and L. McLerran, Nucl. Phys. **A708**, 327 (2002).
[37] A. H. Mueller and D. N. Triantafyllopoulos, Nucl. Phys. **B640**, 331 (2002).
[38] C. Contreras, E. Levin, and R. Meneses, J. High Energy Phys. 10 (2014) 138.
[39] V. S. Fadin and L. N. Lipatov, Phys. Lett. B **429**, 127 (1998); M. Ciafaloni and G. Camici, Phys. Lett. B **430**, 349 (1998).
[40] G. P. Salam, J. High Energy Phys. 07 (1998) 019; M. Ciafaloni, D. Colferai, and G. P. Salam, Phys. Rev. D **60**, 114036 (1999); M. Ciafaloni, D. Colferai, G. P. Salam, and A. M. Stasto, Phys. Rev. D **68**, 114003 (2003).
[41] D. N. Triantafyllopoulos, Nucl. Phys. **B648**, 293 (2003).
[42] V. A. Khoze, A. D. Martin, M. G. Ryskin, and W. J. Stirling, Phys. Rev. D **70**, 074013 (2004).
[43] L. V. Gribov, E. M. Levin, and M. G. Ryskin, Phys. Rep. **100**, 1 (1983).
[44] S. Munier and R. B. Peschanski, Phys. Rev. D **70**, 077503 (2004); **69**, 034008 (2004); Phys. Rev. Lett. **91**, 232001 (2003).
[45] I. Gradstein and I. Ryzhik, *Table of Integrals, Series, and Products*, 5th ed. (Academic Press, London, 1994).
[46] N. Vandersickel and D. Zwanziger, Phys. Rep. **520**, 175 (2012); J. M. Cornwall, Mod. Phys. Lett. A **28**, 1330035 (2013); J. A. Gracey, J. Phys. A **47**, 445401 (2014); P. J. Silva, D. Dudal, and O. Oliveira, *Proc. Sci.* LATTICE (2013) 366, arXiv:1311.3643.
[47] E. Gotsman, E. Levin, U. Maor, and E. Naftali, Eur. Phys. J. C **14**, 511 (2000).
[48] F. D. Aaron *et al.* (H1 and ZEUS Collaborations), J. High Energy Phys. 01 (2010) 109.
[49] V. Andreev *et al.* (H1 Collaboration), Eur. Phys. J. C **74**, 2814 (2014); F. D. Aaron *et al.* (H1 Collaboration), Phys. Lett. B **665**, 139 (2008).
[50] H. Abramowicz *et al.* (ZEUS Collaboration), Phys. Rev. D **90**, 072002 (2014); S. Chekanov *et al.* (ZEUS Collaboration), Phys. Lett. B **682**, 8 (2009).
[51] H. Abramowicz *et al.* (H1 and ZEUS Collaborations), Eur. Phys. J. C **73**, 2311 (2013).
[52] E. Levin and I. Potashnikova, J. High Energy Phys. 02 (2014) 089; 08 (2010) 112.
[53] E. Iancu, J. D. Madrigal, A. H. Mueller, G. Soyez, and D. N. Triantafyllopoulos, Nucl. Phys. **A956**, 557 (2016); Phys. Lett. B **744**, 293 (2015); **750**, 643 (2015).